06

Anisotropy of surface fracture of sapphire plates with basal orientation upon friction

© *A.O. Pozdnyakov, V.M. Krymov, M.E. Boiko, V.I. Nikolaev*

Ioffe Institute, St. Petersburg, Russia
E-mail: ao.pozd@mail.ioffe.ru

The influence of the anisotropy of the crystal structure of sapphire plates on the process of their mechanical wear has been revealed by using cyclic circular motion of silicon carbide spherical indenter over their surface. It is shown that in this friction geometry, crack formation areas are formed on the basal plane. Their centers are located 120° degrees apart from each other along the perimeter of the annular friction trace. Analysis of the crack distribution enables to determine the orientations of the velocity vector relative to the rhombohedral planes responsible for maximum and minimum wear of the sapphire plate of basal orientation.

Keywords: sapphire, rhombohedral planes, anisotropy, crystal lattice, friction, wear.

Owing to a combination of high melting point, hardness, chemical resistance, and transparency, sapphire crystals have a wide variety of applications; for example, they are used to produce LED substrates and optical devices and as a structural material [1]. Most applications require a smooth surface of sapphire components. This is achieved through mechanical processing, which includes precision grinding and chemical-mechanical polishing. The study of abrasion as one of the modes of mechanical interaction of bodies is of practical importance, since it provides an opportunity to improve the quality and efficiency of mechanical processing of sapphire crystals. The mechanical interaction of a crystal with a harder counterbody is investigated using such techniques as micro- and nanoindentation [2,3], scratching [4,5], and friction of sapphire against counterbodies of various nature and shape in different media [6–10]. However, only a small number of orientations of the velocity vector relative to the crystallographic directions were examined. In addition, diamond pyramids were used in friction experiments performed in the majority of published studies; i.e., the initial contact pressure was high, and sapphire sustained severe damage right at the start of the friction process, which made it difficult to analyze the contact area itself. In the present study, we propose a friction test design that covers all directions perpendicular to the basal axis. This design, where friction proceeds with a continuous and smooth direction variation of the velocity vector of a ball indenter relative to the crystallographic directions of a sapphire plate, is being introduced gradually into current studies on crystal friction [11]. The groove left by a silicon carbide ball moving circularly along the basal face of sapphire was examined.

The tribological setup and the method for measuring and calculating the friction force (F_{fr}) were discussed in detail in [12] (see also the references therein). The setup was modified additionally to implement friction of a ball indenter (Fig. 1, *a*) against a plane surface. Ceramic silicon carbide ball *1* (Fushi^{TM} bearings) 6 mm in diameter was secured in cylindrical holder *2* in such a way that the axis of the ball was $r = 1.5$ mm away from the cylinder rotation axis. Stationary sapphire plate *3* was pressed against the ball by fixed load F_n. The linear velocity at the center of the ball–plane contact area: $V = 2\pi r \nu$ (ν is the ball rotation frequency). Friction force F_{fr} in this setup is calculated from the friction-induced torque of plate *3* that is determined using a strain gauge beam [12]. The hardness values of ceramic silicon carbide and sapphire are comparable and fall within the range of $\sim 20-29$ GPa [1,13]. The estimated maximum values of contact pressure in the approximation of elastic contact between an isotropic ball and a plane (the contact radius is then $a = \left(\frac{3F_n R}{4E^*}\right)^{1/3}$, where E^* is the reduced modulus of elasticity [14]) at the maximum F_n used reach ~ 2.5 GPa. This value is in close agreement with the compression strength of both sapphire [1] and SiC-ceramics [7]. The elastic contact area was as large as ~ 0.01 mm^2. Commercial polished ($R_a \sim 20$ nm) sapphire plates ($10 \times 10 \times 1$ mm) with orientations *c* and *m* were used in experiments. The orientation of crystallographic planes was determined by analyzing conoscopic figures (recorded with a Polam^{TM} polarization microscope) and X-ray diffraction patterns obtained using a DRON UM1.0 diffractometer. Profilometry of the friction path along the ring radius was carried out using a MahrPS10 profilometer. The linear wear intensity ($I_h = h/L$, where h is the groove depth and L is the friction distance in the region of ball–plane contact) was chosen as a measure of wear. The linear dimension in the contact area is comparable to the linear size of the contact spot, which, as a first approximation, is estimated as the diameter of the ball–plane contact spot. Microscopic analysis of the ball tip revealed the
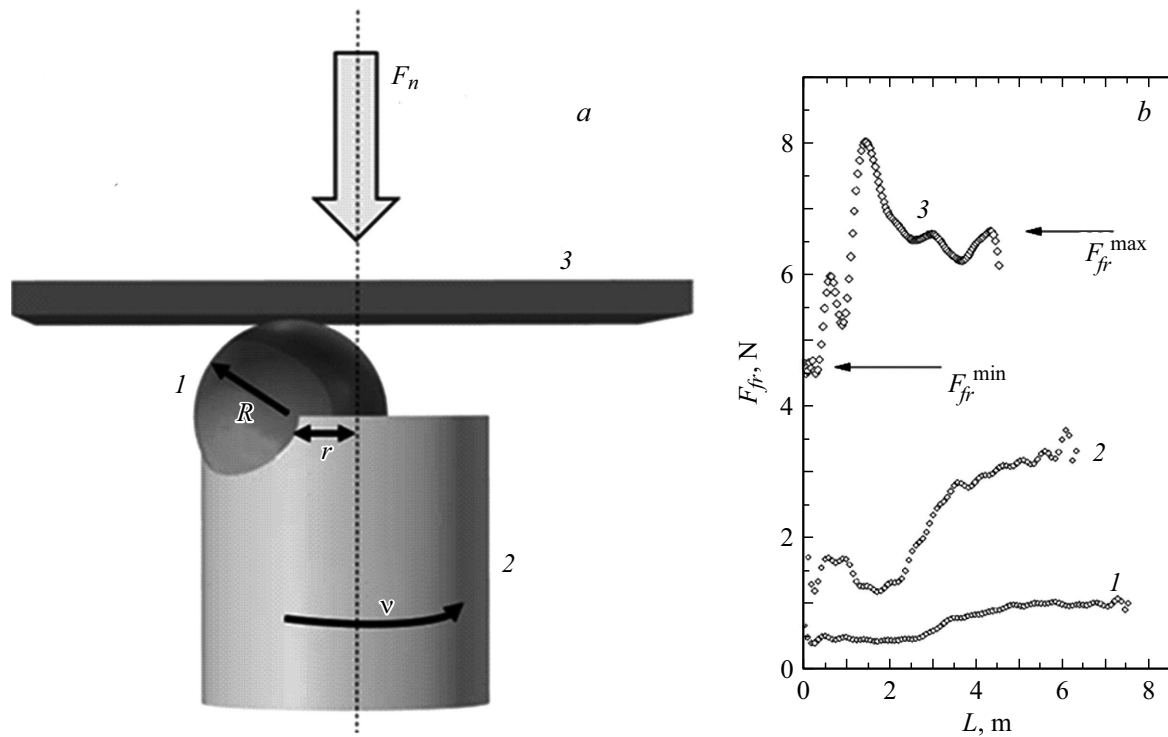
Figure 1. a — Diagram of the ball–plane friction assembly. b — Typical dependences of the friction force on friction distance at different loads: 3 (*1*), 8 (*2*), and 14 N (*3*). Average sliding velocity $V = 0.004$ m/s.

formation of a plateau with a diameter as large as $\sim 500\,\mu$m. This value is a few percent of the overall perimeter of the annular friction trace, which was taken into account in the calculation of I_h. Approximately 30 experimental measurements of F_{fr} with various V $(0-0.0084$ m/s) and F_n $(0-14$ N), where the effects described below were reproduced, were performed. Figure 1, b shows the typical dependences of F_{fr} on friction distance. The key measured effects are the upward shift of the curves with an increase in F_n and the transition of F_{fr} from the lower level to the upper one $(F_{fr}^{\min} \to F_{fr}^{\max})$. These effects are induced by the destruction processes discussed below. Prior to the transition, the friction coefficient $(F_{fr} = \mu F_n)$ is at the level of $0.1-0.2$; after the transition, it assumes a value of $\sim 0.25-0.5$. Note that the $F_{fr}^{\min} \to F_{fr}^{\max}$ transition is accompanied not only by the formation of cracks on the sapphire surface (see below), but also by wear of the ball tip. This implies that the use of a silicon carbide ceramic ball does not allow one to link the F_{fr} behavior unambiguously with wear of the sapphire surface alone.

The formation of an annular friction trace with a radius of 1.5 ± 0.1 mm on the basal plane of sapphire was observed in all experiments (Fig. 2, a). This trace features three extended dark regions positioned $120°$ apart from each other along the perimeter of the ring (i.e., they are characterized by threefold symmetry). They reveal well-defined U-shaped cracks diverging to both sides of the friction path in the direction of ball motion. This crack zone distribution pattern was recorded reliably in experiments

with V and F_n up to ~ 0.005 m/s and 14 N, respectively. At higher values of V and F_n, the damage extended over the entire perimeter of the annular friction trace, and it became difficult to detect cracks in the contact region due to its severe damage. The resulting roughness R_a on the friction path was several micrometers in magnitude. An annular friction trace was also formed in experiments on plates with their surface coinciding with the $m\{1\bar{1}00\}$ plane, but this trace was homogeneous along the entire perimeter and did not feature the discussed cracks. Sapphire crystals tend to cleave along the planes of the morphological rhombohedron that feature threefold symmetry [1]. It is reasonable to assume that the formation of cracks on the friction path is associated with mechanical damage (shear or twinning) along these planes. Archlike U-shaped cracks on the basal plane were noted in one of the first studies on sapphire friction [7], where they were designated as „chevron" cracks without detailing the mechanism of their formation. These cracks were not observed in more recent experiments [4,5] on scratching of sapphire plates with diamond indenters; apparently, this is attributable to the fact that the region under the pyramidal indenter sustained severe damage. Similar cracks were reported in [15], where friction-induced cracks on the surface of diamond were analyzed. They were interpreted as partial cone Hertzian cracks distorted by tensile stress fields behind the indenter.

The change in profiles in the regions between crack clusters did not exceed the sensitivity level of the profilometer, indicating negligible wear in these areas $(I_h \sim 0)$. In the
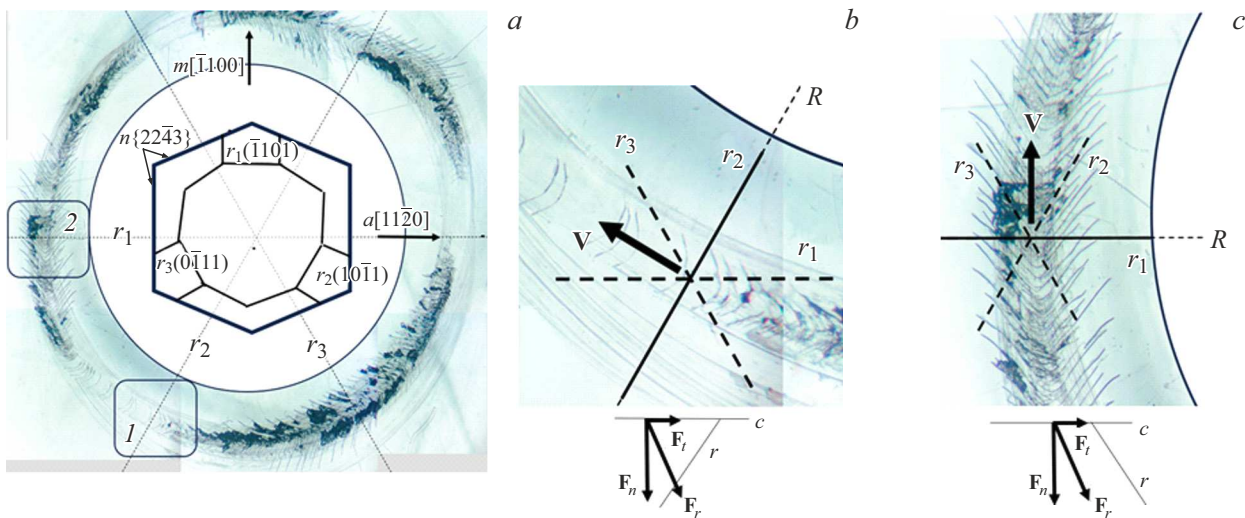
Figure 2. *a* — General view of the annular friction trace on the base plane of a sapphire plate. The plane lattice cell of sapphire is shown in the center. Three dotted lines crossing the entire ring represent the orientation of the lines of intersection of three rhombohedral planes with the basal plane. The ball rotates clockwise. The sliding velocity is $V = 0.005$ m/s, and the load is $F_n = 8$ N. *b* and *c* — Photographic images of regions *1* and *2* in panel *a*. The diagrams show velocity vectors **V**. Three intersecting lines represent the intersections of intersection of rhombohedral planes r_1, r_2, r_3 and the basal plane in these regions. Dotted line *R* indicates the ring radius at the given point. The diagrams of normal compressive force $\mathbf{F}_n$ and shear force $\mathbf{F}_t$ and inclination of planes *r* in these cases are shown below panels *b* and *c*. Sections perpendicular to basal plane *c* and passing through velocity vector **V** are shown.

region of maximum crack density, the profiles had the shape of rough grooves. The maximum estimated I_h values here reached $\sim 10^{-4}$. Note that the area of the contact spot increases in the process of ball–plane friction. This factor is beyond the scope of the present paper. However, the relative increase in linear wear intensity in the region of maximum crack density (compared to that in the regions with minimum crack density) is evident and may be as large as several orders of magnitude. The value of I_h for plates with their surfaces coinciding with plane $m\{1\bar{1}00\}$ did not exceed $\sim 10^{-5}$ at all the examined values of V and F_n, which is consistent with literature data regarding the lower wear resistance of plates with a basal orientation [8,10].

Figures 2, *b* and *c* present enlarged photographic images of cracks in regions *1* and *2* highlighted in Fig. 2, *a*. Three lines intersecting at the point of contact represent the lines of intersection of all three planes (r_1, r_2, and r_3) with the basal plane. Calculations of the Schmid factor and numerical calculations of stresses during indentation of the basal plane reveal threefold symmetry of the maximum probability of fracture along rhombohedral planes, which was confirmed in indentation experiments by the emergence of three cracks intersecting the contact area and oriented at an angle of $120°$ relative to each other [3.16]. In the case of friction, the observed pattern of crack growth is modified significantly. The arrows in Figs. 2, *b* and *c* represent vectors **V** in the regions under consideration. They are tangent to the ring, i.e., they are directed perpendicular to the radius of the annular friction trace (dotted line *R*). It is evident that the linear density of cracks and their shape depend strongly on the relative orientation of vector **V** and the crystallographic

orientation of the crystal. The variation of length of lateral cracks on the right and left sides of the friction path is also noteworthy. For example, the cracks on the right side of the path are longer in the bottom area of the region shown in Fig. 2, *c*. The crack lengths are approximately equal in the middle of the region; as the slider moves further, cracks on the left side become longer (at the top in Fig. 2, *c*). This type of distribution of lateral cracks along the perimeter of the annular friction trace was reproduced reliably in all three regions of crack accumulation, wherein only the specific rhombohedral plane along which crack growth is initiated changes successively in $120°$ intervals. Note that a rough estimate of the shear stress by the value of F_{fr} prior to the $F_{fr}^{\min} \to F_{fr}^{\max}$ transition (several N) with the use of the elastic contact area yields a value below 1 GPa, which is comparable with the level of shear stress characteristic of twinning and shear along rhombohedral planes [3,16]. It may be assumed that other crystal planes (e.g., the $n\{22\bar{4}3\}$ family; Fig. 2, *a*) become involved in fracture and start to provide an additional contribution to the overall wear mechanism as F_n and V grow further.

The kinematic diagrams of orientation of the shear force ($\mathbf{F}_t$) collinear to velocity vector **V**, normal load $\mathbf{F}_n$, and resulting vector $\mathbf{F}_r$ and the relative positions of basal plane *c* and planes *r* are shown at the bottom of Figs. 2, *b* and *c*. Sections perpendicular to basal plane *c* and passing through velocity vector **V** (or $\mathbf{F}_t$) are presented. In the diagram shown in Fig. 2, *b*, resulting vector $\mathbf{F}_r$ is close to the normal of rhombohedral plane r_2; i.e., the resulting chipping force reduces the probability of formation (in this example, along intersection line r_2) and growth (along intersection

lines r_1 and r_3) of cracks. This is evidenced by their low linear density along the perimeter of the ring and the lack of lateral cracks. In the case of the kinematic diagram shown in Fig. 2, c, lateral cracks have a significantly higher linear density; they are elongated and deviate less significantly from the intersection lines (in this example, r_2 and r_3), and the U-shaped initial section is shortened. The direction of vector $\mathbf{F}_r$ in this case is close to the direction along rhombohedral plane r_1. This leads to an increase in chipping stress and the probability of crack formation and growth. The non-uniformity of crack lengths relative to the direction of shear force vector $\mathbf{F}_t$ may be governed by the component of this vector directed along the line of intersection of planes r_2 (Fig. 2, b) and r_1 (Fig. 2, c) with the basal plane, which will affect the level of tensile and compressive stresses in the plate in these directions. The effects described above were reproduced in all three regions of crack accumulation, and the X-ray diffraction analysis data on plate orientations were in excellent agreement with the discussed diagrams. This provides an opportunity to determine the position of rhombohedral planes by analyzing the patterns of crack distribution.

Thus, crystallographic directions of maximum and minimum wear of a sapphire plate of basal orientation in friction against a silicon carbide ball in circular cyclic motion along its surface were revealed. New information regarding the mechanism of formation and growth of cracks on the surface of sapphire plates in the process of friction was obtained. The minimum and maximum wear intensity in different directions was estimated, and the determined values fell within the range of $0-10^{-4}$. The results and the proposed method for obtaining them are of practical value for the study of wear during grinding and polishing of crystals in various crystallographic directions. In addition, these results appear to be important for the development of techniques for production of sapphire substrates for epitaxy and structures that use sapphire-based friction pairs, such as bearings and endoprostheses [1].

Conflict of interest

The authors declare that they have no conflict of interest.

References

[1] E.R. Dobrovinskaya, L.A. Lytvynov, V. Pishchik, *Sapphire: material, manufacturing, applications* (Springer-Verlag, N.Y., 2009). DOI: 10.1007/978-0-387-85695-7

[2] A.B. Sinani, N.K. Dynkin, L.A. Lytvinov, P.V. Konevsky, E.P. Andreev, Bull. Russ. Acad. Sci. Phys., **73**, 1380 (2009). DOI: 10.3103/S1062873809100177.

[3] K. Wang, F. Jiang, L. Yan, X. Xu, N. Wang, X. Zha, X. Lu, Q. Wen, Ceram. Int., **45** (6), 7359 (2019). DOI: 10.1016/j.ceramint.2019.01.021

[4] G. He, H. Wu, H. Huang, H. Zhao, J. Mater. Res. Technol., **31**, 3825 (2024). DOI: 10.1016/j.jmrt.2024.07.093

[5] W. Lin, J. Shimizu, L. Zhou, T. Onuki, H. Ojima, Prec. Eng., **73**, 51 (2022). DOI: 10.1016/j.precisioneng.2021.08.011

[6] R.P. Steijn, J. Appl. Phys., **32** (10), 1951 (1961). DOI: 10.1063/1.1728269

[7] C.H. Riesz, H.S. Weber, Wear, **7** (1), 67 (1964). DOI: 10.1016/0043-1648(64)90079-1

[8] Yu.A. Fadin, O.F. Kireenko, V.M. Krymov, S.P. Nikanorov, Bull. Russ. Acad. Sci. Phys., **73**, 1383 (2009). DOI: 10.3103/S1062873809100189.

[9] A.B. Voloshin, L.A. Litvinov, E.L. Ostrovskaya, T.P. Yukhno, I.V. Timchenko, Mater. Elektron. Tekh., No. 1, 16 (2004) (in Russian).

[10] Q. Luo, J. Lu, X. Xu, F. Jiang, Ceram. Int., **43** (18), 16178 (2017). DOI: 10.1016/j.ceramint.2017.08.194

[11] T. Wang, Q. Yan, Q. Xiong, J. Lin, J. Lu, J. Pan, Mater. Sci. Semicond. Process., **172**, 108059 (2024). DOI: 10.1016/j.mssp.2023.108059

[12] A.O. Pozdnyakov, L. Syanshun, E.B. Sedakova, J. Frict, Wear, **45**, 24 (2024). DOI: 10.3103/S1068366624700041

[13] https://www.preciseceramic.com/products/silicon-carbide-sic.html

[14] V.L. Popov, M. Heß, E. Willert, *Handbook of contact mechanics, exact solutions of axisymmetric contact problems* (Springer, Berlin−Heidelberg, 2019). DOI: 10.1007/978-3-662-58709-6

[15] B.R. Lawn, Proc. Roy. Soc. Lond. A., **299**, 307 (1967). DOI: 10.1098/rspa.1967.0138

[16] R. Nowak, T. Manninen, K. Heiskanen, T. Sekino, A. Hikasa, K. Niihara, T. Takagi, Appl. Phys. Lett., **83** (25), 5214 (2003). DOI: 10.1063/1.1635983

Translated by D.Safin